J. Plasma Phys. (2024), *vol*. 90, 175900201
Published by Cambridge University Press
doi:10.1017/S0022377824000539

Hybrid electrostatic waves in linearized gravity

Chinmoy Bhattacharjee [1],† **and David J. Stark** [2,3]

[1]Department of Physics, New York Institute of Technology, Old Westbury, NY 11568, USA

[2]Plasma Theory and Applications, Los Alamos National Laboratory, Los Alamos, NM 87545, USA

[3]Department of Physics, College of William & Mary, Williamsburg, VA 23185, USA

(Received 10 October 2023; revised 28 March 2024; accepted 3 April 2024)

Linearized gravity around a rotating black hole or compact object introduces the concept of a gravitomagnetic field, which originates from the matter–current in the rotating object. Plasma in proximity to this object is subsequently subjected to motion guided by this gravitomagnetic term (where mass serves as the effective charge) in addition to the conventional magnetic field. Such an interplay of fields complicates the accessible plasma waves of the system and thus merits exploration to delineate this interplay, to identify any observable signatures of the gravitomagnetic field in weakly magnetized systems, and to motivate future numerical work in a fully relativistic setting where the effects may be stronger. In this work we analyse the dispersion of the upper and lower hybrid electrostatic waves in a plasma immersed in both magnetic and gravitomagnetic fields. In particular, we discuss the effective augmentation or cancellation of the two fields under the right conditions for the upper hybrid wave. In contrast, the lower hybrid wave experiences a frequency up-shift from the gravitomagnetic field regardless of whether it is parallel or antiparallel to the magnetic field for the studied field strengths.

Keywords: astrophysical plasmas, plasma waves, plasma dynamics

1. Introduction

When the spacetime near a black hole or compact star is stationary, one can slice the spacetime into three-dimensional space plus one-dimensional time. This approach is dictated by the stationarity of background spacetime and is known as '$3+1$' splitting (Thorne & Macdonald 1982; Thorne, Price & MacDonald 1986). The three-dimensional space is considered as curved rather than Euclidean and is the spatial part of background metric $g_{\mu\nu}$ in an appropriately chosen coordinate system. The metric of a stationary spacetime in the Boyer–Lindquist coordinate can be written as

$$\mathrm{d}s^2 = -\alpha^2 c^2\,\mathrm{d}t^2 + g_{ij}(\mathrm{d}x^j + \mathcal{N}^j\,\mathrm{d}t)(\mathrm{d}x^i + \mathcal{N}^i\,\mathrm{d}t), \tag{1.1}$$

where α is the lapse function, $\mathcal{N}^i$ is the shift vector and g^{ij} is the spatial metric. In the weak gravity and low velocity ($v \ll c$) limit, one can define two gravitational potentials in this space: the traditional Newtonian gravitational scalar potential Φ_g and a vector potential $\boldsymbol{A}_g = c\boldsymbol{\mathcal{N}}$ known as the gravitomagnetic potential.

† Email address for correspondence: usa.chinmoy@gmail.com

These two potentials can be used to define the following two vector fields:

$$\boldsymbol{g} = -\boldsymbol{\nabla} \ln \alpha, \quad \boldsymbol{B}_g = \boldsymbol{\nabla} \times \boldsymbol{A}_g, \tag{1.2a,b}$$

where $\boldsymbol{g}$ is the Newtonian gravitational field (gravitoelectric) and $\boldsymbol{B}_g$ is a 'magnetic'-type gravity known as the gravitomagnetic field, respectively (Braginsky, Caves & Thorne 1977; Hobson, Efstathiou & Lasenby 2006; Bhattacharjee & Stark 2021). The analogy of these two fields with the electromagnetic ones becomes more obvious when the $3+1$ split is applied to a weakly gravitating, rotating body. It can be shown that in the weak gravity limit, the Einstein field equations for this object can be cast into a form similar to the time-independent Maxwell's equations,

$$\boldsymbol{\nabla} \cdot \boldsymbol{g} = -4\pi\rho_m, \quad \boldsymbol{\nabla} \cdot \boldsymbol{B}_g = 0, \tag{1.3a,b}$$

$$\boldsymbol{\nabla} \times \boldsymbol{g} = 0, \quad \boldsymbol{\nabla} \times \boldsymbol{B}_g = -\frac{4\pi G}{c}\boldsymbol{J}_m, \tag{1.4a,b}$$

where ρ_m and $\boldsymbol{J}_m$ are the mass and mass-current density of the gravitating body, respectively. It should be noted that the minus sign indicates gravity is attractive.

One of the major predictions of gravitomagnetism is the precession of the gyroscope near a large rotating mass, also known as the frame-dragging effect. This notably has been confirmed by the Gravity Probe B experiments in 2005 (Everitt *et al.* 2011). Recently, the pulsar PSR J1141-6545 circling a white dwarf has been detected to show a long-term orbital drift by measuring the pulses emanated from the pulsar to an accuracy to within 100 μs over a period of nearly 20 years (Krishnan *et al.* 2020). In the context of black hole accretion disk theory, the gravitomagnetic force is predicted to cause differential precession of the disk. This force acting in conjunction with the viscous force can cause the accretion disk to have a warped structure, a phenomenon known as the Bardeen–Petterson effect (Bardeen & Petterson 1975; Kumar & Pringle 1985; Thorne *et al.* 1986; Nelson & Papaloizou 2000; Lei, Zhang & Gao 2012; Nealon, Price & Nixon 2015). Observationally, this effect can cause the astrophysical jets emanating from the black holes to change their orientations rapidly (Miller-Jones *et al.* 2019).

In this article, we study the impact of the gravitomagnetic field on the plasma waves in the accretion disk around a rotating black hole or compact object. Plasmas in the accretion disk are often magnetized, but the presence of a background gravitomagnetic field can change the characteristics of the plasma wave modes. The traditional approach is to solve the fully general relativistic (GR) system including the Einstein's field equation and relativistic plasma equation of motion. The analytical complexities of such a calculation makes it impossible to understand the results in terms of classical plasma wave modes. Here, we are primarily motivated to uncover possible first-order corrections to the classical plasma wave modes, which can serve as a benchmark and motivation for a much more detailed GR calculation in stronger gravity in the future. As a part of this scheme, we investigate two electrostatic wave modes important to astrophysical plasma phenomena: upper hybrid and lower hybrid modes in the presence of both magnetic and gravitomagnetic fields. In a magnetized plasma, these electrostatic modes travel perpendicular to the background magnetic field, which is often oriented along the axis of rotation. In this study, we allow the gravitomagnetic field to be parallel or antiparallel to the background field to best elucidate the interplay of the two fields. One can expect that the presence of a gravitomagnetic field in a magnetized plasma can alter the characteristics of these two modes and potentially have observational effects on the electromagnetic spectrum, plasma heating and magnetic reconnection processes in the accretion disk near a

https://doi.org/10.1017/S0022377824000539 Published online by Cambridge University Press

compact object under the right conditions (Roy & Lakhina 1985; Bell & Ngo 1990; Lesch 1991; Pécseli *et al.* 1996; Cairns & McMillan 2005; Wallace *et al.* 2010; Liang *et al.* 2013; Chen *et al.* 2020).

We present the background on plasma dynamics in a gravitomagnetic field in the first section. Next, we derive the dispersion relations for both modes the upper and lower hybrid waves. We conclude with a discussion of the application of these results to accretion disk plasmas.

2. Plasma dynamics

In this article, we consider the plasma dynamics in an accretion disk near a slowly rotating compact object such as a black hole or neutron star. The slowly rotating object can be characterized by its mass M and spin parameter $a = J/Mc \ll 1$ (in the units of half-Schwarzschild-radius $r_g = GM/c^2$), in which G is the gravitational constant, c is the speed of light and J is the angular momentum (Misner, Thorne & Wheeler 1973; Thorne *et al.* 1986; Hobson *et al.* 2006). Moreover, the plasmas we consider here are (i) located at larger radii from the Schwarzschild radius ($r \gg 2r_g = GM/c^2$) and (ii) moving with a bulk velocity much lower than the speed of light ($v \ll c$).

The accretion disk considered here is assumed to be unmagnetized initially, implying the magnetorotational instability is not operational yet. It has been shown in the pure hydrodynamical set-up that angular momentum transport can still be sustained in these types of disks (Fragile & Anninos 2005; Paoletti *et al.* 2012; Ghosh & Mukhopadhyay 2021). Instead of investigating the plasma dynamics of the accretion disk which has settled to its equilibrium structure, we concentrate on the time scale when seed magnetic fields are being generated in the disk by mechanisms such as Biermann battery, spacetime curvature drive, gravitomagnetic drive, etc. (Mahajan & Yoshida 2011; Bhattacharjee, Das & Mahajan 2015; Bhattacharjee & Stark 2021). Therefore, our analysis of wave modes will be limited to the range of seed magnetic field values in the accretion disk or where there are relatively unmagnetized regions of a larger structure.

Under these approximations, the plasma dynamics of individual species (labelled s) can be represented by the equation of motion and the continuity equation, respectively (Thorne *et al.* 1986; Bhattacharjee & Stark 2021),

$$m_s n_s \left(\frac{\partial}{\partial t} + \boldsymbol{v}_s \cdot \boldsymbol{\nabla}\right) \boldsymbol{v}_i = -\boldsymbol{\nabla} p_s + q_s n_s \boldsymbol{E} + \frac{q_s n_s}{c} (\boldsymbol{v}_s + \boldsymbol{\mathcal{N}}) \times \boldsymbol{B} + \frac{m_s n_s}{c} (\boldsymbol{v}_s \times \boldsymbol{B}_g) + m_s n_s \boldsymbol{g}, \tag{2.1}$$

$$\frac{\partial n_s}{\partial t} + \boldsymbol{\nabla} \cdot (n_s \boldsymbol{v}_s) = 0, \tag{2.2}$$

where m_s is the species mass, n_s is the plasma number density, $\boldsymbol{v}_s$ is the velocity, p_s is the pressure, $\boldsymbol{E}$ is the electric field, $\boldsymbol{B}$ is the magnetic field and $\boldsymbol{g} = -\boldsymbol{\nabla}\Phi_G$ is the Newtonian gravitational acceleration. It should be noted here that the two new terms containing ($\boldsymbol{\mathcal{N}} \times \boldsymbol{B}$) and ($\boldsymbol{v}_s \times \boldsymbol{B}_g$) on the right-hand side of (2.1) are corrections due to rotating spacetime with $\boldsymbol{B}_g$ representing the 'magnetic'-type gravitomagnetic field and its corresponding vector potential $\boldsymbol{A}_g = c\boldsymbol{\mathcal{N}}$. The shift vector is divergence-free $\boldsymbol{\nabla} \cdot \boldsymbol{\mathcal{N}} = 0$ in the Boyer–Lindquist coordinate (Thorne *et al.* 1986) and can be interpreted as the angular velocity of zero angular momentum observers (also known as fiducial observers) in a stationary background spacetime. It should be noted here that the Lorentz force term in (2.1) has a coupling between the magnetic field and gravity through the term $\boldsymbol{\mathcal{N}} \times \boldsymbol{B}$. The $m_s n_s (\boldsymbol{v}_s/c \times \boldsymbol{B}_g)$ term on the right-hand side of (2.1) is a new force that can be attributed

https://doi.org/10.1017/S0022377824000539 Published online by Cambridge University Press

to the frame-dragging caused by the spacetime's intrinsic rotation. The consequence of this new force has been studied quite extensively in the context of fluid dynamics in black hole accretion disks and is known as the Bardeen–Petterson effect (Bardeen & Petterson 1975; Nelson & Papaloizou 2000).

In an axisymmetric stationary spacetime near a weakly rotating object, the gravitomagnetic field takes the following form:

$$\boldsymbol{B}_g = \frac{2G}{c}\left(\frac{\boldsymbol{J}}{R^3} - \frac{3(\boldsymbol{J}\cdot\boldsymbol{r})\boldsymbol{r}}{R^5}\right) \tag{2.3}$$

with its corresponding vector potential

$$\boldsymbol{A}_g = \frac{2G}{c}\frac{\boldsymbol{J}\times\boldsymbol{r}}{R^3}. \tag{2.4}$$

Here, $R = \sqrt{r^2 + z^2}$ is the distance to the plasma element from the central mass, and $\boldsymbol{r}$ is associated with the cylindrical coordinate system (r, ϕ, z). If we take the angular momentum of the object $\boldsymbol{J}$ along the z-axis and assume the disk to be thin ($z \ll r$), then (2.3) becomes

$$\boldsymbol{B}_g = \frac{2G}{c}\frac{\boldsymbol{J}}{r^3}, \tag{2.5}$$

which can be expressed in the following normalized form:

$$\boldsymbol{B}_g = \frac{2\tilde{a}c^2}{r_g}\frac{1}{\tilde{r}^3}\hat{z}. \tag{2.6}$$

Here we have used the following normalizations: spin parameter $\tilde{a} = J/Mcr_g$ and radial distance $\tilde{r} = r/r_g$. The spin parameter $\tilde{a}$ can have a maximum value of 1. However, in order for the gravitomagnetic approximation to be valid, we consider cases where spin parameter $|\tilde{a}| < 0.3$. This specific range has also been confirmed to produce the frame-dragging effect when modelling the accretion disk near a rotating object by means of Newtonian physics (Chakrabarti & Khanna 1992).

3. Electrostatic wave modes in electron–ion plasma

To obtain the electrostatic wave modes in an incompressible electron–ion plasma, we need (2.1), (2.2) and Poisson's equation,

$$\nabla\cdot\boldsymbol{E} = \sum_s n_s q_s. \tag{3.1}$$

First, we assume the background electric field $\boldsymbol{E}_0 = 0$ and a uniform background plasma density, i.e. $\nabla n_{0s} = 0$. Next, we look for wave modes in the electron–ion plasma with wavevector $\boldsymbol{k} = k\hat{x}$ in a background magnetic and gravitomagnetic fields $(\boldsymbol{B}_0, \boldsymbol{B}_g)$ $||\hat{z}$. Then, using the following perturbations: $n = n_{0s} + \delta n_s$, $\boldsymbol{E} = \delta\boldsymbol{E}||\boldsymbol{k}$ and $\boldsymbol{v}_s = \boldsymbol{v}_{0s} + \delta\boldsymbol{v}_s$, we

https://doi.org/10.1017/S0022377824000539 Published online by Cambridge University Press

linearize (2.1), (2.2) and (3.1) and solve for the dispersion relation of the system, yielding

$$1 - \frac{\omega_{\mathrm{pe}}^2}{(\omega - \boldsymbol{k}\cdot\boldsymbol{v}_{0e})^2 - \gamma_e k_b T_e k^2/m_e - \tilde{\omega}_e^2/m_e^2} - \frac{\omega_{\mathrm{pi}}^2}{(\omega - \boldsymbol{k}\cdot\boldsymbol{v}_{0i})^2 - \gamma_i k_b T_i k^2/m_i - \tilde{\omega}_i^2/m_i^2} = 0, \tag{3.2}$$

where T_e, T_i stand for electron and ion temperature, respectively; electron plasma frequency $\omega_{\mathrm{pe}} = \sqrt{4\pi n_e q_e^2/m_e}$, ion plasma frequency $\omega_{\mathrm{pi}} = \sqrt{4\pi n_i q_i^2/m_i}$, $\tilde{\omega}_s = (q_s/cB_0 + m_s\omega_g)$ is the modified cyclotron frequency for both species, gravitomagnetic frequency $\omega_g = B_g/c$ and γ is the adiabatic index for each species.

For simplicity in isolating the new physics, for the rest of this article we assume background flow $v_{0s} \approx 0$ for both species and write (3.2) as

$$1 - \frac{1}{\tilde{\omega}^2 - \beta_e^2 - \tilde{\omega}_{\mathrm{ce}}^2(1-\epsilon_e)^2} - \frac{1}{Z^2}\frac{\alpha}{\tilde{\omega}^2 - \tilde{\gamma}\alpha\beta_e^2 - \alpha^2 Z^2\tilde{\omega}_{\mathrm{ce}}^2\left(1 + \frac{1}{\alpha Z}\epsilon_e\right)^2} = 0. \tag{3.3}$$

In (3.3), we have used the following normalizations: $\tilde{\omega} = \omega/\omega_{\mathrm{pe}}$, $\tilde{\omega}_{\mathrm{ce}} = \omega_{\mathrm{ce}}/\omega_p$, $\alpha = m_e/m_i$, $\beta_e = \sqrt{\gamma_e}(kv_{\mathrm{th}(e)}/\omega_{\mathrm{pe}})$, $\tilde{\gamma} = \gamma_i/\gamma_e$, $q_i = Ze$, $\epsilon_e = \omega_g/|\omega_{\mathrm{ce}}|$, $\epsilon_i = 1/Z\alpha\,\epsilon_e$ where thermal velocity for both species $v_{\mathrm{the}(s)} = \sqrt{k_b T_s/m_s}$, Z is the atomic number, and electron cyclotron frequency $|\omega_{\mathrm{ce}}| = eB/m_e c$.

In (3.3), it should be noted that both the second and third terms on the left-hand side are modified by the factors $(1-\epsilon_e)^2$ and $(1 + (1/\alpha Z)\epsilon_e)^2$, respectively. These two terms are explicit contributions from gravitomagnetism with the factor $\epsilon_e = \omega_g/|\omega_{\mathrm{ce}}|$ measuring the relative strength between the gravitomagnetic and magnetic field. In the absence of a gravitomagnetic field, (3.3) becomes the standard dispersion relation for electrostatic waves in a magnetized electron–ion plasma.

Figure 1(*a*) plots the dispersion relation for different values of ϵ_e, where the traditional upper hybrid oscillation is represented by a black dotted line. For the rest of the article, we assume a hydrogen plasma for simplicity. For different values of ϵ_e, we notice different vertical shifts in the frequency plot from the $\epsilon_e = 0$ case (black line). As $|\epsilon_e|$ increases from 0, the frequency at $\beta_e = 0$ shifts from the classical upper hybrid oscillation in a direction depending on the sign of ϵ_e. For $\epsilon_e < 0$, the frequency is pushed above the classical value, whereas for $\epsilon_e > 0$, the frequency is pushed below it. In the latter case, we see that setting $\epsilon_e = 1.0$ results in a starting frequency at ω_{pe}. In this case, there is an effective cancellation of the magnetic and gravitomagnetic fields, resulting in $\omega_s = 0$. Here the wave behaves as a standard unmagnetized electron plasma wave. We note, however, that for $\epsilon_e > 1.0$, the gravitomagnetic field will then no longer be cancelled by the magnetic field and the frequency will once again rise above the plasma frequency. At $\epsilon_e = 2.0$, the mode will match the case of $\epsilon_e = 0$, but now the mode is primarily influenced by the gravitomagnetic field as opposed to the magnetic field.

The interplay between the magnetic and gravitomagnetic fields can further be visualized by constructing a $\omega_{\mathrm{ce}}, \omega_g$ phase space plot showing the cutoff frequency $\omega(\beta_e = 0)$ for each combination. Figure 1(*b*) gives ω_g and ω_{ce} each in the range of -1 to 1 (still normalized to ω_{pe}) and the colour coding is $\omega(\beta_e = 0)$ using the same normalization. The diagonal blue region is where both fields are parallel and equal in magnitude in the plasma ($\epsilon_e = 1$); however, because the electron has a negative charge in the magnetic field and a positive effective charge (its mass) in a gravitomagnetic field, the effect of the fields

https://doi.org/10.1017/S0022377824000539 Published online by Cambridge University Press

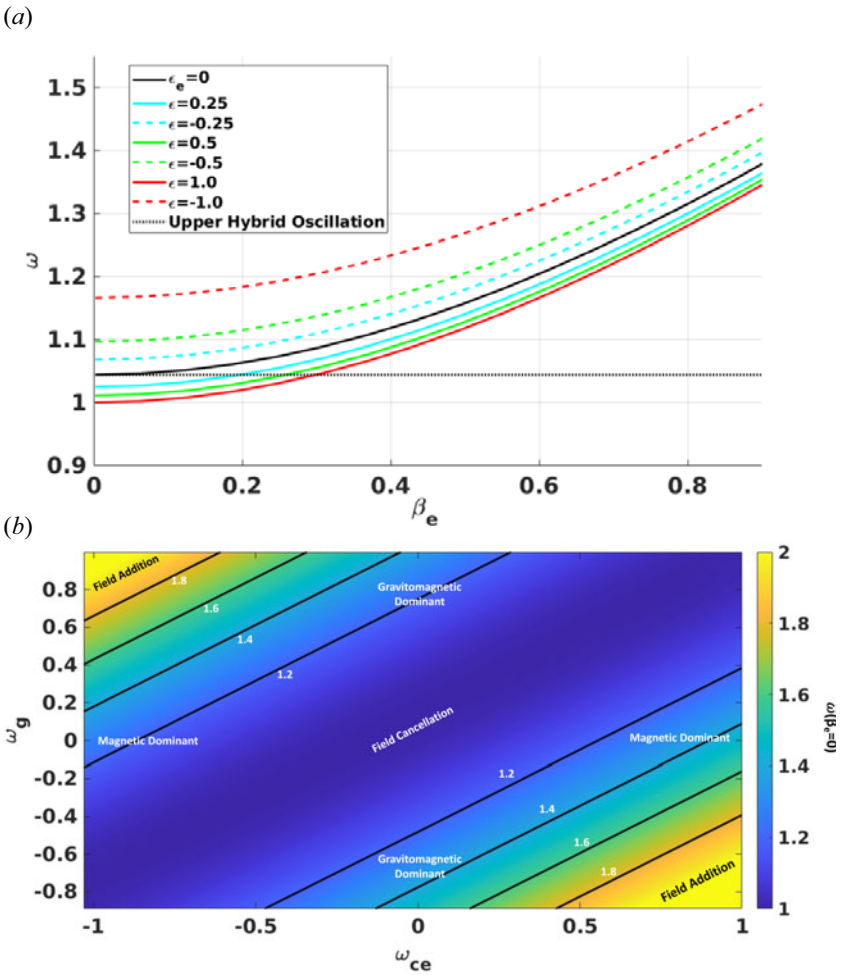

FIGURE 1. (*a*) Plot of ω versus β for the upper hybrid wave with modifications due to different ϵ_e values. The classical upper hybrid oscillation is given in the dashed black line. (*b*) Plot of the cutoff frequency $\omega(\beta = 0)$ in $\omega_{\rm ce}$, ω_g phase space. Contours are given in black and additional annotation shows the relative contributions of the gravitomagnetic and magnetic fields.

on the electron will cancel. This implies that a purely magnetized plasma near a weakly rotating object can sustain a Langmuir wave perpendicular to the background field under the right conditions, which is possible because both magnetic and gravitomagnetic fields cancel in their impact on electrons.

In contrast, the yellow regions at the upper left-hand and lower right-hand corners indicate that magnetic and gravitomagnetic fields are colinear ($\epsilon_e = -1$) in the plasma. Here the force on an electron in the gravitomagnetic field will be in the same direction as that from the magnetic field, so the effective magnetic field or cyclotron frequency will increase. Contours of $\omega(\beta_e = 0)$ are denoted in black. The remaining four regions in the phase space can be distinguished based on the relative magnitudes of the background magnetic and gravitomagnetic fields within the plasma. This implies unmagnetized or weakly magnetized plasmas near the object can sustain electrostatic wave modes mimicking those seen in magnetized plasma.

https://doi.org/10.1017/S0022377824000539 Published online by Cambridge University Press

Figure 2(*a*) shows the lower hybrid wave dispersion for different values of ϵ_e. In contrast to the high-frequency modes, we do not see any significant differences in the dispersion relations between ϵ_e values of the same magnitude but opposite sign. As the classical lower hybrid oscillation frequency depends on both the electron and ion cyclotron frequencies, there will always be one species where the gravitomagnetic field effectively increases the cyclotron frequency and one species where it effectively reduces this frequency. Under the assumption of $\epsilon_e \gg \alpha$, the lower hybrid oscillation (setting $\beta_e = 0$) is

$$\omega_{\mathrm{LH}}^2 \sim \frac{\alpha\omega_{\mathrm{ce}}^2}{1+\omega_{\mathrm{ce}}^2} + \epsilon_e^2\omega_{\mathrm{ce}}^2 \tag{3.4}$$

to lowest order in α and ϵ_e. The dashed horizontal line shows the classical lower hybrid oscillation frequency, and all tested values of ϵ_e cause an increase from this value due to the ϵ_e^2 dependence in the equation.

In figure 2(*b*), we once again plot the phase space of the gravitomagnetic and cyclotron frequencies and colour code by the cutoff frequency $\omega(\beta_e = 0)$, this time for the lower hybrid wave. When the magnitude of the magnetic field increases, the relative gravitomagnetic contribution diminishes. We note that no field cancellation is observed in this lower frequency mode in the plasma under this set of plasma conditions. The contour lines (black) form a unique island-type structure for lower values of both magnetic and gravitomagnetic fields, but the contours become mostly vertical in the case of $|\omega_{\mathrm{ce}}| \gg |\omega_g|$.

4. Discussion and conclusion

We have presented the dispersion relation of electrostatic waves in a warm electron–ion plasma travelling perpendicular to background magnetic and gravitomagnetic fields. The plasma is assumed to be non-relativistic and located in an accretion disk near a weakly rotating astrophysical object. Though the system is non-relativistic, the first-order effect from GR in the plasma dynamics is in the form of a gravitomagnetic force. As a result, the combination of both magnetic and gravitomagnetic fields alters the standard cyclotron frequency, and this results in modifications to the classical upper and lower hybrid waves. The relative orientation of magnetic and gravitomagnetic fields permits the existence of pure Langmuir waves in this magnetized plasma under the conditions of gravitomagnetic cancellation. The existence of these modes can potentially be verified in observations during the propagation of electromagnetic transmissions in the accretion disk (Chen 2012). This prediction becomes obvious when we ignore the ion dynamics and consider the cold plasma limit. In this limit, (3.2) can be rewritten as

$$\frac{(\omega_{\mathrm{ce}}+\omega_g)^2}{\omega^2} = 1 - \frac{4\pi nq^2}{m\omega^2}, \tag{4.1}$$

where $\omega_g = B_g/c$ is the gravitomagnetic frequency. As the plasma density varies in the disk, the electromagnetic transmission through the plasma varies as well based on the frequency spectrum. This profile should be different from the standard upper hybrid frequency – to which the electromagnetic waves can couple – because of the existence of gravitomagnetism and depends on the strength and relative orientation of the background magnetic and gravitomagnetic fields. This can serve as one of the tests for the GR prediction of frame dragging in the non-relativistic limit, in additional to serving as a potential indirect diagnostic of the rotation of the object.

However, since the regime in which the approximations are valid necessitates a relatively weak gravitomagnetic field, the objects and structures where this can be useful requires

https://doi.org/10.1017/S0022377824000539 Published online by Cambridge University Press

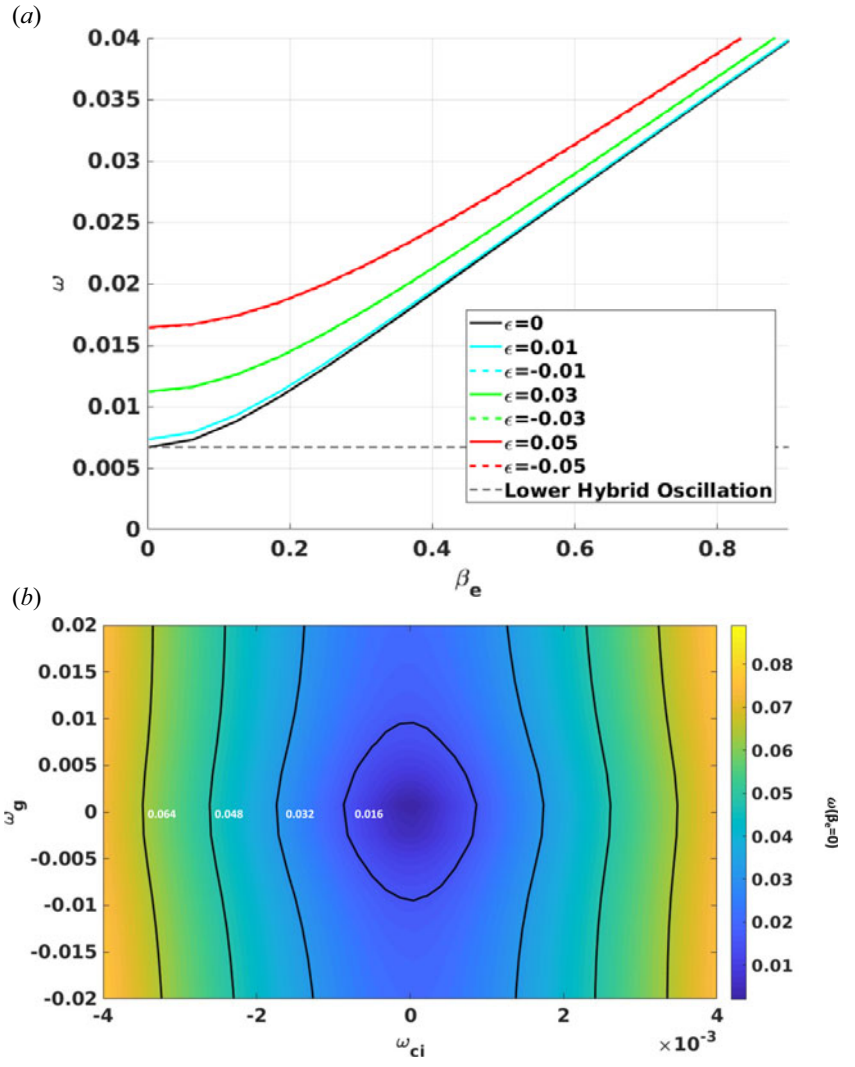

FIGURE 2. (*a*) Plot of ω versus β for the lower hybrid wave with modifications due to different ϵ_e values. The classical lower hybrid oscillation is given in the dashed black line. (*b*) Plot of the cutoff frequency $\omega(\beta_e = 0)$ in $\omega_{\rm ce}$, ω_g phase space. Contours are given in black.

careful consideration. We can estimate ω_g as

$$\omega_g \sim \frac{\tilde{a} \times 10^5}{\tilde{M}\tilde{r}^3}, \tag{4.2}$$

introducing $\tilde{M}$ as the mass of the object in units of the solar mass. From this we see that increasing ω_g for a fixed $\tilde{r}$ requires smaller masses, so stellar mass black holes or neutron stars are more likely to lead to something observable. Looking then at ω_c, we find

$$\omega_c \sim 1.76 \times 10^8 \beta, \tag{4.3}$$

https://doi.org/10.1017/S0022377824000539 Published online by Cambridge University Press

in which β is the magnetic field (in gauss) at the corresponding location $\tilde{r}$ from the object. To have $\omega_g \sim \omega_c$ (or $\epsilon_e \sim 1$), therefore

$$\beta \sim \frac{1}{176}\frac{\tilde{a}}{\tilde{M}\tilde{r}^3}. \tag{4.4}$$

Even with optimal gravitomagnetic parameters of $\tilde{a} = 0.3$, $\tilde{M} = 5$ and $\tilde{r} = 40$ – while still remaining in the regime of validity of the gravitomagnetic approximations – we find that the magnetic field for $\epsilon_e \sim 1$ is $\sim 10^{-9}$ G, which may be most appropriate for primordial black hole systems (Safarzadeh 2018; Araya *et al.* 2021; Papanikolaou & Gourgouliatos 2023) or other seed-field systems discussed in § 2. Since smaller ϵ_e values still alter the dispersion of the hybrid modes, more modern systems with larger magnetic fields may potentially have measurable gravitomagnetic fields. However, we would still be limited to relatively unmagnetized regions of accretion disks, which exist in such systems with complex structures (Riffert 1980), and in particular when there are oscillatory field structures (Bhattacharjee, Feng & Stark 2018). Furthermore, extended observation times would be required to reach frequency resolution necessary to observe any gravitomagnetic shifts.

This derivation was performed in the post-Newtonian limit, but if this were done in a full GR setting, one would be able to look at conditions closer to the object where these effects would be considerably stronger. While this calculation does not directly apply in such a regime, we hope that it serves as a motivation and benchmark for future simulation studies (likely requiring a GR particle-in-cell code), where greater specifics of observable signatures can be better explored.

When ion dynamics plays an important role, we found that the lower hybrid waves also experience modifications from gravitomagnetism. However, these modes change in a fundamentally different way compared with the upper hybrid modes, as we do not see field cancellation for our plasma conditions, even if the relative orientation between these two fields changes. It should be noted that as the relative strength of the gravitomagnetic field increases, the cutoff frequency increases as well. This, in turn, alters the spectrum of waves with which the lower hybrid waves can interact, on both electron and ion scales (Liu, Chen & Ma 2021). Lower hybrid waves can efficiently transfer energy from the perpendicular motions of ions to the parallel motions of electrons or *vice versa*, either accelerating particles or heating them (Verdon *et al.* 2008). What our results indicate is that gravity (through gravitomagnetic contributions to the lower hybrid wave mode) can play a non-negligible role in this energy transfer mechanism in ion and electron length scales, which will be explored later in detail. Moreover, the behaviour of these modes in the small magnitude field limit is quite different from their higher frequency counterparts. A further analysis is necessary to explore this behaviour in the low-frequency regime, which will be addressed in future work.

Acknowledgements

Editor R. Blandford thanks the referees for their advice in evaluating this article.

Funding

C.B.'s work is supported by the NYIT Institutional Support of Research and Creativity (ISRC) Grants.

Declaration of interests

The authors report no conflict of interest.

https://doi.org/10.1017/S0022377824000539 Published online by Cambridge University Press

REFERENCES

Araya, I.J., Rubio, M.E., San Martin, M., Stasyszyn, F.A., Padilla, N.D., Magana, J. & Sureda, J. 2021 Magnetic field generation from pbh distributions. *Mon. Not. R. Astron. Soc*. **503** (3), 4387–4399.

Bardeen, J.M. & Petterson, J.A. 1975 The lense-thirring effect and accretion disks around Kerr black holes. *Astrophys. J*. **195**, L65.

Bell, T.F. & Ngo, H.D. 1990 Electrostatic lower hybrid waves excited by electromagnetic whistler mode waves scattering from planar magnetic-field-aligned plasma density irregularities. *J. Geophys. Res*. **95** (A1), 149–172.

Bhattacharjee, C., Das, R. & Mahajan, S.M. 2015 Novel mechanism for vorticity generation in black-hole accretion disks. *Phys. Rev.* D **91** (12), 123005.

Bhattacharjee, C., Feng, J.C. & Stark, D.J. 2018 Surveying the implications of generalized vortical dynamics in curved space–time. *Mon. Not. R. Astron. Soc*. **481** (1), 206–216.

Bhattacharjee, C. & Stark, D.J. 2021 Gravitomagnetic vorticity generation in black hole accretion discs: a potential spatial constraint on plasma flow stability. *Mon. Not. R. Astron. Soc*. **508** (1), 414–420.

Braginsky, V.B., Caves, C.M. & Thorne, K.S. 1977 Laboratory experiments to test relativistic gravity. *Phys. Rev.* D **15** (8), 2047.

Cairns, I.H. & McMillan, B.F. 2005 Electron acceleration by lower hybrid waves in magnetic reconnection regions. *Phys. Plasmas* **12** (10). doi: 10.1063/1.2080567

Chakrabarti, S.K. & Khanna, R. 1992 A Newtonian description of the geometry around a rotating black hole. *Mon. Not. R. Astron. Soc*. **256** (2), 300–306.

Chen, F.F. 2012 *Introduction to Plasma Physics*. Springer Science & Business Media.

Chen, L.-J., *et al.* 2020 Lower-hybrid drift waves driving electron nongyrotropic heating and vortical flows in a magnetic reconnection layer. *Phys. Rev. Lett*. **125** (2), 025103.

Everitt, C.W.F., *et al.* 2011 Gravity probe B: final results of a space experiment to test general relativity. *Phys. Rev. Lett*. **106** (22), 221101.

Fragile, P.C. & Anninos, P. 2005 Hydrodynamic simulations of tilted thick-disk accretion onto a Kerr black hole. *Astrophys. J*. **623** (1), 347.

Ghosh, S. & Mukhopadhyay, B. 2021 Origin of hydrodynamic instability from noise: from laboratory flow to accretion disk. *Phys. Rev. Fluids* **6** (1), 013903.

Hobson, M.P., Efstathiou, G.P. & Lasenby, A.N. 2006 *General Relativity: An Introduction for Physicists*. Cambridge University Press.

Krishnan, V.V., *et al.* 2020 Lense–thirring frame dragging induced by a fast-rotating white dwarf in a binary pulsar system. *Science* **367** (6477), 577–580.

Kumar, S. & Pringle, J.E. 1985 Twisted accretion discs: the Bardeen–Petterson effect. *Mon. Not. R. Astron. Soc*. **213** (3), 435–442.

Lei, W.-H., Zhang, B. & Gao, H. 2012 Frame dragging, disk warping, jet precessing, and dipped X-ray light curve of Sw J1644 + 57. *Astrophys. J*. **762** (2), 98.

Lesch, H 1991 Electron heating in accretion disks of active galactic nuclei-on the formation of ion-supported tori. *Astron. Astrophys*. **245**, 48–56.

Liang, Y., *et al.* 2013 Magnetic topology changes induced by lower hybrid waves and their profound effect on edge-localized modes in the east tokamak. *Phys. Rev. Lett*. **110** (23), 235002.

Liu, X., Chen, L. & Ma, Q. 2021 A statistical study of lower hybrid waves in the Earth's magnetosphere by Van Allen probes. *Geophys. Res. Lett*. **48** (10), e2021GL093168.

Mahajan, S.M. & Yoshida, Z. 2011 Relativistic generation of vortex and magnetic field. *Phys. Plasmas* **18** (5). doi: 10.1063/1.3566081

Miller-Jones, J.C.A., *et al.* 2019 A rapidly changing jet orientation in the stellar-mass black-hole system V404 Cygni. *Nature* **569** (7756), 374–377.

Misner, C.W., Thorne, K.S. & Wheeler, A.J. 1973 *Gravitation*. W.H. Freeman and Company.

Nealon, R., Price, D.J. & Nixon, C.J. 2015 On the Bardeen–Petterson effect in black hole accretion discs. *Mon. Not. R. Astron. Soc*. **448** (2), 1526–1540.

NELSON, R.P. & PAPALOIZOU, J.C.B. 2000 Hydrodynamic simulations of the Bardeen–Petterson effect. *Mon. Not. R. Astron. Soc*. **315** (3), 570–586.

PAOLETTI, M.S., VAN GILS, D.P.M., DUBRULLE, B., SUN, C., LOHSE, D. & LATHROP, D.P. 2012 Angular momentum transport and turbulence in laboratory models of Keplerian flows. *Astron. Astrophys*. **547**, A64.

PAPANIKOLAOU, T. & GOURGOULIATOS, K.N. 2023 Primordial magnetic field generation via primordial black hole disks. *Phys. Rev.* D **107** (10), 103532.

PÉCSELI, H.L., IRANPOUR, K., HOLTER, Ø., LYBEKK, B., HOLTET, J., TRULSEN, J., ERIKSSON, A. & HOLBACK, B. 1996 Lower hybrid wave cavities detected by the FREJA satellite. *J. Geophys. Res*. **101** (A3), 5299–5316.

RIFFERT, H. 1980 Pulsating X-ray sources: the oblique dipole configuration. *Astrophys. Space Sci*. **71**, 195–201.

ROY, M. & LAKHINA, G.S. 1985 Lower hybrid wave model for aurora. *Astrophys. Space Sci*. **117** (1), 111–120.

SAFARZADEH, M. 2018 Primordial black holes as seeds of magnetic fields in the universe. *Mon. Not. R. Astron. Soc*. **479** (1), 315–318.

THORNE, K.S. & MACDONALD, D. 1982 Electrodynamics in curved spacetime: 3 + 1 formulation. *Mon. Not. R. Astron. Soc*. **198** (2), 339–343.

THORNE, K.S., PRICE, R.H. & MACDONALD, D.A. 1986 *Black Holes: The Membrane Paradigm*. Yale University Press.

VERDON, A.L., CAIRNS, I.H., MELROSE, D.B. & ROBINSON, P.A. 2008 Properties of lower hybrid waves. *Proc. Intl Astronom. Union* **4** (S257), 569–573.

WALLACE, G.M., *et al.* 2010 Absorption of lower hybrid waves in the scrape off layer of a diverted tokamak. *Phys. Plasmas* **17** (8). doi: 10.1063/1.3465662